Architecture of Columnar Nacre, and Implications for Its Formation Mechanism

Rebecca A. Metzler,[1] Mike Abrecht,[2] Ronke M. Olabisi,[1] Daniel Ariosa,[3] Christopher J. Johnson,[4] Bradley H. Frazer,[2] Susan N. Coppersmith,[1] and P. U. P. A. Gilbert[1,*]

[1]*Department of Physics, University of Wisconsin, Madison, Wisconsin 53706, USA*
[2]*Synchrotron Radiation Center, 3731 Schneider Drive, Stoughton, Wisconsin 53589, USA*
[3]*Institute for the Physics of Complex Matter, EPF-Lausanne, CH-1015 Switzerland*
[4]*Program in Cellular and Molecular Biology & Department of Animal Health and Biomedical Sciences, School of Veterinary Medicine, University of Wisconsin, Madison, Wisconsin 53706, USA*

(Received 30 March 2007; published 29 June 2007)

We analyze the structure of *Haliotis rufescens* nacre, or mother-of-pearl, using synchrotron spectromicroscopy and x-ray absorption near-edge structure spectroscopy. We observe imaging contrast between adjacent individual nacre tablets, arising because different tablets have different crystal orientations with respect to the radiation's polarization vector. Comparing previous data and our new data with models for columnar nacre growth, we find the data are most consistent with a model in which nacre tablets are nucleated by randomly distributed sites in the organic matrix layers.

DOI: 10.1103/PhysRevLett.98.268102 PACS numbers: 87.68.+z, 61.10.Ht

Biominerals in general [1–6] and nacre, or mother-of-pearl, in particular [7–10] attract the attention of scientists in material science, biology, and mineralogy as well as physics because of their remarkable mechanical properties and their incompletely elucidated formation mechanisms. Nacre is a composite of alternating layers of organic matrix (OM) and aragonite, 30 and 400–500 nm thick [11,12], respectively. Each aragonite layer consists of 5–10 μm wide tablets of irregular polygonal shape that completely fill the space between preformed OM layers.

We investigate the structure of nacre using new experimental measurements and address possible mechanisms of nacre formation with theoretical simulations. Our experimental data demonstrate c-axis orientation disorder of nacre tablets across different nacre layers, and we show that characterizing this disorder yields insight into nacre's formation mechanism.

We use x-ray photoelectron emission spectromicroscopy (X-PEEM) or simply synchrotron spectromicroscopy [13] to obtain information about the orientation of nacre tablets. X-PEEM is a surface sensitive technique (probing depth of 3 nm at the carbon K-edge [14]) that enables imaging and extraction of spectroscopic information from a single layer of nacre tablets, or from a polished cross section including many layers. X-ray absorption near-edge structure (XANES) [15] spectra were extracted from individual tablets, and compared with simulated spectra for aragonite crystals. Our bulk x-ray diffraction data from the same abalone shell are consistent with previously reported data [12,16] and with the spectromicroscopy results reported here, which were acquired on the VLS-PGM undulator beam line at the SRC [17].

Figure 1 presents X-PEEM data of nacre tablets acquired on the Spectromicroscope for the PHotoelectron Imaging of Nanostructures with X-rays (SPHINX) X-PEEM [1,13]. The carbon map of Fig. 1(a) represents, with different gray levels, the intensity of the peak at 290.3 eV [18] in the C K-edge XANES spectra have different nacre tablets, as shown in Fig. 1(b). The 290.3 eV peak corresponds to the $C1s \rightarrow \pi^*$ transition of the CO bond (hereafter referred to as the π^* peak) [15,19]. Synchrotron radiation is linearly polarized in the orbit plane. Under such illumination, the intensity of the π^* peak depends on the crystallographic orientation of each nacre tablet with respect to the polarization, as detailed below. A map of nacre tablets exhibiting such high contrast between adjacent tablets was previously observed with dark field TEM imaging for the intracrystalline OM [10], but never for the aragonite crystal orientation. Interestingly, the oxygen π^* peak exhibits the same variation, and maps as well as carbon does [see Fig. 1(c)], while Ca distributions appear completely homogeneous [see Fig. 1(d)], as do all direct images of nacre acquired at monochromatic energies outside the narrow energy region around the π^* peak. The contrast observed in the maps of Fig. 1 is the first observation of x-ray linear dichroism, a polarization-dependent phenomenon widely studied in materials physics [20,21], in a natural biomineral.

Our simulated XANES spectra obtained using the FEFF software package [22,23], as well as our experimental XANES measurements on single aragonite crystals at different orientations, confirm that the intensity variation of Fig. 1(a) arises because the polar angle θ, the angle between the c-axis and the polarization vector, differs for each tablet, and the c-axes of different tablets are not all parallel to each other but misoriented. The contrast must arise from polar orientation variations, because the relative intensities of the peaks cannot vary when only the azimuthal angle is varied, and aragonite has triangular symmetry in the ab-plane [15]. X-ray diffraction measurements on nacre by us and by others [16,24] indicate that c-axis orientation in nacre varies by $\pm 11^\circ$ over centimeter length

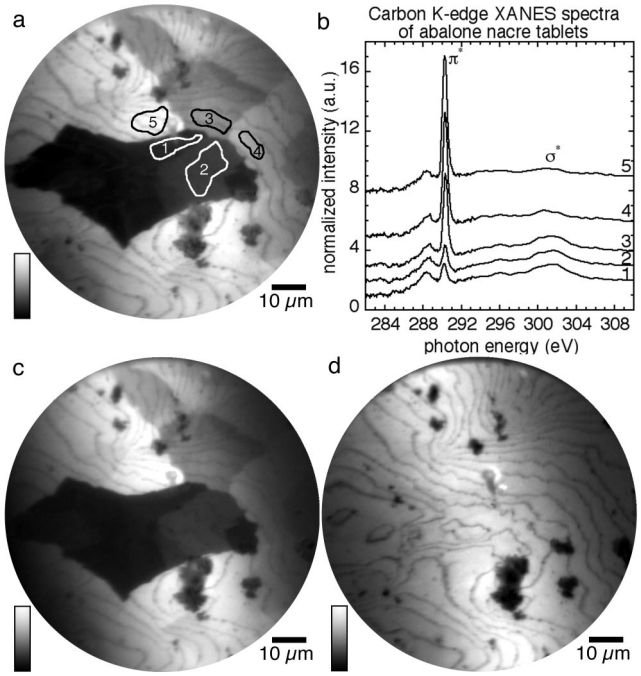

FIG. 1. X-ray linear dichroism generates contrast in nacre tablets. In this nacre sample the growth direction was perpendicular to the image plane; thus, the nacre layers are almost parallel to the surface, and appear as contour lines where they are not flat. The polarization vector is 16° from the growth direction; the microscope geometry is described in [13]. (a) Distribution map of the carbon π^*/σ^* signal on the polished surface of red abalone nacre. The map was obtained by digital ratio of two X-PEEM micrographs acquired with SPHINX at 290.3 and 302 eV. The immediately adjacent tablets 1 and 5 exhibit the highest dichroic contrast. (b) Carbon K-edge XANES spectra extracted from the correspondingly labeled regions in (a). The π^* peak at 290.3 eV and the σ^* peak at 302 eV have anticorrelated intensities that change dramatically from tablet to tablet. Each spectrum is normalized to the beam line background and to a linear background fit above 310 eV, so the pre- and post-edge intensities, below 283 eV and above 310 eV are 0 and 1, respectively. These spectra were all acquired simultaneously from a stack of 200 images, and confirmed in a repeated acquisition. (c) Distribution map of oxygen π^*/pre-edge signal at 534 and 531.7 eV, respectively, showing the same dichroic contrast as the carbon map. (d) Distribution map of calcium, showing only the Ca-poor OM layers, and no crystal tablet contrast.

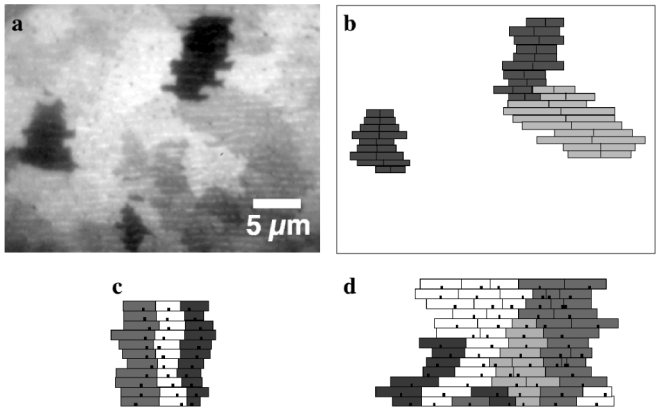

FIG. 2. (a) X-PEEM oxygen π^* map of a polished cross section of red abalone nacre, obtained by ratio of 534 and 518 eV images. The angle between the growth direction and the polarization vector was ~61°. The growth direction in this sample was 60° from the normal to the polished nacre surface, so the layer thickness appears to be greater than 500 nm. (b) Outlines of the tablets in (a) from 3 distinct nacre co-oriented columns, bisected by vertical lines. (c)–(d) Results from two-dimensional models of abalone nacre growth. Both models assume randomly distributed nucleation sites in the first layer (bottom, in each model), that the orientation of the tablet nucleated at a given location in row $n + 1$ is the same as that of the tablet in row n, directly below the nucleation site, and assume that horizontal growth occurs at a uniform rate, and is only arrested when tablets become contiguous. Co-oriented tablets are indicated by the same gray level. (c) Tablet nucleation in layer $n + 1$ occurs within a 0.7 μm diameter of the nucleation site of the underlying tablet in layer n (the maximum diameter of the tablet in layer n when it reaches a height of 0.4–0.5 μm, based upon the growth rate of nacre tablets found by Lin and Meyers [25]). (d) Nucleation sites for tablets in layer $n + 1$ are distributed uniformly and randomly on the OM layer separating layers n and $n + 1$.

scales, while there is no long-range order in ab orientation. The X-PEEM results yield the new information that the polar variability occurs on the scale of individual tablets.

The spectromicroscopy data for a cross section of red abalone nacre shown in Fig. 2(a) demonstrate that tablet orientation is conserved across approximately 10 layers. This result is consistent across different shells, and different areas of the same shell, with 40 as the maximum number of co-oriented tablets observed in red abalone. Figure 2(a) demonstrates that the growth direction of nacre cannot be identified with the c-axis of nacre tablets, as usually assumed, because the c-axis is oriented differently in neighboring columns of tablets.

Figure 2(b) shows that a vertical line bisecting each tablet within a column of co-oriented tablets does not necessarily align with the column axis. Rather, several co-oriented tablets are stacked, with each successive tablet ($n + 1$, $n + 2$, etc.) offset in one direction [right or left in Fig. 2(b)] relative to tablet n. Other columns of tablets are stacked approximately along the vertical growth direction. For simplicity, hereafter we refer to this appearance as "skewed columns."

We now discuss modeling results that show how our experimental results yield insight into possible growth mechanisms of nacre. Recent results of Nudelman *et al.* report a single nucleation site per tablet [7], and optical micrographs of individual layers of nacre tablets in abalone (not shown) yield patterns of tablets that are consistent with the hypotheses that each tablet has a single nucleation site, that the nucleation sites are randomly distributed in

the ab-plane, the tablet growth is isotropic in the ab-plane, and growth only stops at confluence. The simplistic assumption of isotropic growth in the ab-plane is conceivable for either growth of aragonite crystals from solution ions or growth of aragonite tablets via nanograin aggregation [10,26,27].

A simple two-dimensional model yields insight into how different nucleating mechanisms affect the resulting organization of successive layers. Our growth models all start with an initial condition of randomly distributed nucleation sites for the first growth layer and arbitrarily assigned crystallographic orientations for each tablet in the first growth layer. We assume that a tablet nucleated in layer $n + 1$ has the same crystallographic orientation as the tablet in layer n, directly below the nucleation site. Figure 2(c) shows growth when the nucleation site in layer $n + 1$ is restricted to be close to the nucleation site of a tablet below it in row n, which corresponds to nucleation occurring soon after the tablet in layer n reaches its full height [11,28]. This model results in aligned columns that do not resemble the skewed columns observed in bulk nacre [Fig. 2(a)].

Figure 2(d) shows growth when the nucleation sites for layer $n + 1$ are chosen at random locations anywhere within the OM layer between tablet n and $n + 1$, with the orientation of the tablet in row $n + 1$ the same as the tablet in row n, directly below the nucleation site. This model generates columns that are qualitatively similar to those measured experimentally [Fig. 2(a)].

Our results are consistent with a growth mechanism in which the OM layers are formed first, with randomly distributed nucleation sites that have no associated crystallographic orientation. Once a tablet in layer n reaches a nucleation site, the latter nucleates a tablet in layer $n + 1$ with the same orientation.

We propose that nucleation sites are preexisting in the OM layers before crystal nucleation and growth, but do not become active until growth has proceeded to an appropriate stage. We propose the following mechanism to describe nucleation sites consisting of active organic molecules: on side n of the OM layer, a STOP molecule arrests aragonite growth for tablet n along the growth direction, while its counterpart START molecule on the other side of the same OM layer is activated and nucleates a new aragonite tablet $n + 1$. It is possible that a templating mechanism exists, in which organic molecules alone determine the crystal orientation of aragonite, as described by Gilbert *et al.* [1]; alternatively, crystal orientation could be determined by the underlying crystal directly. Specifically, the ring-shaped nucleation sites observed by Nudelman *et al.* [7] would simply have pores at their center through which the underlying crystal grows [28,29]. The latter could be either the aragonite crystal or the organic crystal observed by Rousseau *et al.* [10]. Regardless of the mechanism by which the crystal orientation is templated, the time sequence must be enforced. This can be achieved with either or both the START/STOP molecules, and a porous region in the OM layer as the "nucleation site." These scenarios are both fully consistent with the recent proposal by Addadi *et al.* that amorphous calcium carbonate may be a precursor to aragonite in nacre tablet formation [30]. In this scenario, growth of aragonite tablets at the expense of amorphous calcium carbonate is expected, and crystal orientation determined by a separate templating mechanism.

To summarize, we have shown that aragonite exhibits x-ray linear dichroism. Exploiting this novel contrast mechanism, we have used XANES and X-PEEM spectromicroscopy to resolve individual tablets in pristine bulk nacre. It appears that individual tablets indeed behave as single crystals under polarized x-ray illumination, and the nanograins observed by Rousseau *et al.* in *Pinctada maxima* [10] and Li *et al.* in *Haliotis rufescens* [26] are all co-oriented within each tablet. The c-axes of individual aragonite tablets in nacre are not oriented parallel to the growth direction, and there are significant differences in the orientation of the c-axes of neighboring tablets. Furthermore, we reveal that there are columns of co-oriented tablets, with the number of tablets per co-oriented column varying between 1 and 40. These observations allow us to discriminate among possible formation mechanisms for nacre growth. The model that best resembles bulk columnar nacre has randomly distributed nucleation sites, preformed on organic matrix layers before tablet nucleation and growth. The resulting scenario reconciles apparently discrepant lines of evidence, and encompasses the present results and all other data currently available on the mystery of abalone nacre formation.

We are grateful to Mark Friesen for his assistance with MATLAB simulations, to Ben Gilbert for his advice on FEFF simulations, and to Andreas Scholl for useful discussions on dichroism. This work was supported by NSF Grants No. PHY-0523905, No. PHY-0646018, and No. CHE-0613972, UW-Graduate School Romnes and Vilas Grants to P. U. P. A. G., and NSF Grants No. DMR-0209630 to S. N. C. The experiments were performed at the UW-SRC, supported by NSF Grant No. DMR-0537588.

*Previously published as Gelsomina De Stasio.
Corresponding author.
pupa@physics.wisc.edu

[1] P. U. P. A. Gilbert, B. H. Frazer, and M. Abrecht, in *Molecular Geomicrobiology*, edited by J. F. Banfield, K. H. Nealson, and J. Cervini-Silva (Mineralogical Soc. Am., Washington DC, 2005), Vol. 59, p. 157.
[2] R. Daw, Nature (London) **427**, 691 (2004).
[3] S. Mann and G. A. Ozin, Nature (London) **382**, 313 (1996).
[4] A. M. Belcher *et al.*, Nature (London) **381**, 56 (1996).

[5] S. Weiner, I. Sagi, and L. Addadi, Science **309**, 1027 (2005).
[6] C. S. Chan and G. De Stasio *et al.*, Science **303**, 1656 (2004); D. Fortin, Science **303**, 1618 (2004).
[7] F. Nudelman, B. A. Gotliv, L. Addadi, and S. Weiner, J. Struct. Biol. **153**, 176 (2006).
[8] I. M. Weiss, V. Schonitzer, N. Eichner, and M. Sumper, FEBS Lett. **580**, 1846 (2006).
[9] N. Nassif *et al.*, Proc. Natl. Acad. Sci. U.S.A. **102**, 12 653 (2005).
[10] M. Rousseau *et al.*, Biomaterials **26**, 6254 (2005).
[11] S. Blank *et al.*, J. Microsc. **212**, 280 (2003).
[12] C. M. Zaremba *et al.*, Chem. Mater. **8**, 679 (1996).
[13] B. H. Frazer, M. Girasole, L. M. Wiese, T. Franz, and G. De Stasio, Ultramicroscopy **99**, 87 (2004).
[14] B. H. Frazer, B. Gilbert, B. R. Sonderegger, and G. De Stasio, Surf. Sci. **537**, 161 (2003).
[15] J. Stohr, *NEXAFS Spectroscopy* (Springer-Verlag, Berlin, 1992).
[16] S. W. Wise, Eclogae geologicae Helvetiae **63**, 775 (1970).
[17] R. Reininger, G. De Stasio, M. Bissen, and M. Severson, *SRI 2003*, edited by T. Warwick *et al.*, AIP Conf. Proc. No. 705 (AIP, New York, 2004), p. 305.
[18] This and all other energies reported hereafter have a ± 0.1 eV error due to variability from sample to sample.
[19] R. J. Madix, J. L. Solomon, and J. Stohr, Surf. Sci. **197**, L253 (1988).
[20] J. Stöhr *et al.*, Phys. Rev. Lett. **47**, 381 (1981).
[21] J. Stöhr *et al.*, Science **292**, 2299 (2001).
[22] The FEFF simulations were done using the crystal coordinates for geologic aragonite at http://cars9.uchicago.edu/atomsdb/CaCO3-ara.inp. The linear polarization and its direction with respect to the sample were specified using ELLIPTICITY and POLARIZATION cards in the FEFF input file. C and O *K*-edge XANES spectra were simulated at polar angles varying from $0°-90°$. Both C and O spectra exhibit dichroism.
[23] A. L. Ankudinov *et al.*, Phys. Rev. B **65**, 104107 (2002).
[24] S. Mann, *Biomineralization* (Oxford University, New York, 2001).
[25] A. Lin and M. A. Meyers, Mater. Sci. Eng. A **390**, 27 (2005).
[26] X. Li, Z.-H. Xu, and R. Wang, Nano Lett. **6**, 2301 (2006).
[27] R. L. Penn and J. F. Banfield, Am. Mineral. **83**, 1077 (1998).
[28] L. Addadi and S. Weiner, Nature (London) **389**, 912 (1997).
[29] T. Schäffer *et al.*, Chem. Mater. **9**, 1731 (1997).
[30] L. Addadi, D. Joester, F. Nudelman, and S. Weiner, Chem. Eur. J. **12**, 980 (2006).